

An Improved Split-Step Wavelet Transform Method for Anomalous Radio Wave Propagation Modeling

Asif IQBAL, Varun JEOTI

Dept. of Electrical and Electronics Engineering, Universiti Teknologi Petronas, Tronoh, Perak, 31750, Malaysia

asif.iqbal@msn.com, varun.jeoti@petronas.com.my

Abstract. *An Anomalous tropospheric propagation caused by ducting phenomenon is a major problem in wireless communication. Thus, it is important to study the behavior of radio wave propagation in tropospheric ducts. The Parabolic Wave Equation (PWE) method is considered most reliable to model anomalous radio wave propagation. In this work, an improved Split Step Wavelet transform Method (SSWM) is presented to solve PWE for the modeling of tropospheric propagation over finite and infinite conductive surfaces. A large number of numerical experiments are carried out to validate the performance of the proposed algorithm. Developed algorithm is compared with previously published techniques; Wavelet Galerkin Method (WGM) and Split-Step Fourier transform Method (SSFM). A very good agreement is found between SSWM and published techniques. It is also observed that the proposed algorithm is about six times faster than WGM and provide more details of propagation effects as compared to SSFM.*

Keywords

Radio wave propagation, parabolic equation method, Split Step Fourier transform, split step wavelet transform, wavelet Galerkin, tropospheric duct.

1. Introduction

Due to the varying nature of refractive index in troposphere, the radio waves do not follow the straight path as they do in free space. Since the radio refractive index varies spatially and diurnally, it is necessary to carefully take it into account before designing a wireless communication system. The gradient of refractive index causes the formation of layers or ducts. When radio waves are channeled through these ducts, they behave differently from normal environment. This non-standard propagation is also referred to as anomalous propagation. Due to ducting phenomenon and earth surface profile, radio wave is affected by reflection, refraction and diffraction mechanisms. Since the occurrence of these mechanisms is localized and geometry specific, it is very difficult to develop a uniform model to accurately predict the propagation in such varying environments. Various an-

alytical and numerical models have been developed to forecast the behavior of radio wave propagation in such environments. In numerical model, most reliable and widely used technique for tropospheric radio wave propagation modeling is the Parabolic Wave Equation (PWE) method [1]. In 1946, the PWE method was first used for tropospheric radio wave propagation modeling by Leonovich and Fock [2] and then, in 1984, it was extended [3] for the case of a two dimensional inhomogeneous atmosphere. With the passage of time, different versions of PWE are derived for many other areas [4], [5], [6], [7].

PWE is derived from the Helmholtz equation by taking into account only the forward propagation. As a full-wave model, PWE models have certain unique advantages. First, PWE can handle the refraction and diffraction effects simultaneously. Therefore, it is not only simple in calculations, the accuracy level is also high. Second, PWE can efficiently model the electromagnetic field distribution over irregular surfaces under non-uniform distribution of the refractive index of atmospheric structure. Third, PWE model results in iterative algorithms. Therefore, PWE model can be used for regional forecast of propagation path loss.

The vast application and extensive research shows the relative importance of the PWE model [4],[5], [6], [8]. It should be noted that the robustness of PWE solution depends on numerical technique used. For a given application, the selection of best numerical technique is warranted to provide the accurate results.

Due to complex boundary conditions and channel properties over earth surface, the rigorous solution of PWE is a challenging task and it has been investigated by many researchers for many years. PWE became an essential tool for modeling wave propagation after the development of SSFM by Tappert and Hardin [8]. SSFM takes the advantage of computationally efficient Fast Fourier Transform (FFT) algorithm [9], [10], [11]. In SSFM, diffraction and refraction effects are treated separately while it also allows larger range increments. The later property makes this algorithm attractive for large domain solutions. On the other hand, Finite difference (FD) method and Finite Element (FE) Method are also quite popular for solving PWE [4], [12], [13], [14], [15], [16]. Effective boundary handling makes FD and FE methods attractive to the numerical solution of PWE. However,

FD and FE methods are resource hungry in term of memory and processing for non-standard atmospheric conditions.

Besides the conventional numerical techniques mentioned above, another strong contender for the numerical solutions of Partial Differential Equations (PDEs) is the wavelet based methods. Briefly, a wavelet is a short duration oscillatory mathematical function. In 1980s, Morlet and Groszman used a French word *ondette* for these functions. Later, it was translated to wavelet by translating *onde* into wave [17]. Ingrid Daubechies constructed the class of compactly supported scaling and wavelet function in 1988 [18]. In early nineties, the attractive properties of wavelets had drawn researcher attention to the application of wavelets for numerical solution of PDEs. Afterwards, numerous linear and non-linear problems have been solved using wavelet based numerical technique. It was proved that the best localization properties of wavelets lead to efficient numerical method especially for the problem that involves the formation of shock, hurricane and turbulence etc. [19], [20], [21]. Normally, wavelet based techniques can be classified into three types: methods based on scaling function expansion, methods based on wavelet expansion and methods based on wavelet optimized finite differences [22].

Recently authors of this paper have developed a wavelet method based on scaling function expansion namely WGM for the solution of PWE [23]. But from numerical experiments, it is observed that WGM has similar characteristics as FE Method. It does not allow larger range increments for higher frequencies which leads to higher processing load. Due to the computational complexity problem encountered in WGM, the focus is now shifted towards SSWM. SSWM is also one of the popular techniques to model non-linear optical pulse propagation [24], [25]. SSWM is also used for the application of underwater acoustic propagation [26]. It is found that the complexity of SSWM is minimum as compared to SSFM and SSWM is considered to be more accurate and computationally more efficient for large domain solutions. Authors of this paper also showed the feasibility of SSWM for the solution of PWE for Perfectly Electric Conductive (PEC) ground surfaces [27], [28].

In this work, an improved formulation of SSWM is presented. The formulation of [27], [28] is generalized for impedance boundary conditions using Discrete Mixed Fourier Transform (DMFT). Unlike other sub-domain solutions, the proposed method not only allows larger range steps but also provides more accurate solution. It is seen to be as fast as SSFM.

This work mainly focuses on the modeling of tropospheric radio wave propagation under ducting phenomenon using wavelets based numerical technique. The model under consideration is a two-dimensional standard PWE. Furthermore, finitely conductive flat earth surface is assumed under range dependent/independent environment. The propagation path loss is computed for range independent and dependent

environment cases. We also consider standard and ducting atmospheric conditions.

Since this work is still a fundamental research for the application of wavelet to model radio wave propagation, the topics like time dependent PWE, three dimensional (3D) PWE and/or wide angle PWE and experimental validation of proposed path loss propagation model are beyond the scope of this study. The rough surface modeling is also not studied in this work. Only the wavelet methods based on scaling function expansion are employed to solve PWE. Daubechies family of wavelet is used throughout this work. The application of other classes of wavelet and the comparison between different families of wavelet to model radio wave propagation is also beyond the scope of this study.

This paper is organized as follows: Problem formulation of tropospheric boundary value problem is given in section 2. A detailed SSWM formulation is given in section 3. Section 4 includes the numerical implementation of the SSWM algorithm. At the end, results are compared with those from WGM and SSFM for various environment conditions.

2. Problem Statement: Tropospheric Boundary Value Problem

To develop the outline of the method briefly, a fairly simple problem is selected to formulate. The model under consideration here is a two-dimensional standard PWE for the case of Tropospheric radio propagation over flat surfaces. The paraxial form of scalar wave equation in Cartesian coordinates system is given by [1]

$$\frac{\partial^2 u}{\partial z^2} - 2jk_0 \frac{\partial u}{\partial x} + k_0^2(n^2 - 1)u = 0, \quad (1)$$

$$Z_{min} \leq z \leq Z_{max}, x \geq 0$$

where $k_0 = 2\pi/\lambda$ is the wave number in vacuum and m is the modified refractive index. Here, x -axis is the direction of propagation while z -axis is the height above ground level. The geometry of PWE problem for radio wave propagation modeling and range dependant refractivity profiles are illustrated in Fig. 1 (a) and (b) respectively. The limits of height and range axis are defined as; $Z_{min} \leq z \leq Z_{max}$ and $x \geq 0$. The whole domain is discretized into N_z no. of small grids. In Fig. 1, Δx and Δy are the discretizing size for range and height respectively. Bottom surface (Z_{min}) is finite or infinite conductive flat surface while an absorbing layer at the top of 'domain of interest' (Z_{req}). The bottom boundary is flat earth surface.

2.1 Boundary Conditions

Impedence Boundary Conditions:

Equation (1) should satisfy the boundary condition to handle the electromagnetic field at the earth surface. The boundary conditions at surface of a smooth, finitely conducting earth can be approximated by [16]

$$\alpha_1(x) \frac{\partial}{\partial z} u(x, z)|_{z=0} + \alpha_2(x) u(x, z)|_{z=0} = 0 \quad (2)$$

where $\alpha_1(x)$ and $\alpha_2(x)$ are constants. For a perfectly conducting surface, $\alpha_1(x) = 0$ (Dirichlet BC) and $\alpha_2(x) = 0$ (Neumann BC) for horizontal and vertical polarization respectively. For finitely conducting earth surface, $\alpha_1(x) = 1$, while $\alpha_2(x) = (j/\mu_0\omega)\eta$ for horizontal polarization and $\alpha_2(x) = -j\omega\epsilon_s\eta$ for vertical polarization. Here, ϵ_s is the permittivity of the surface medium, μ_0 is the free-space permeability, and ω is the radial frequency.

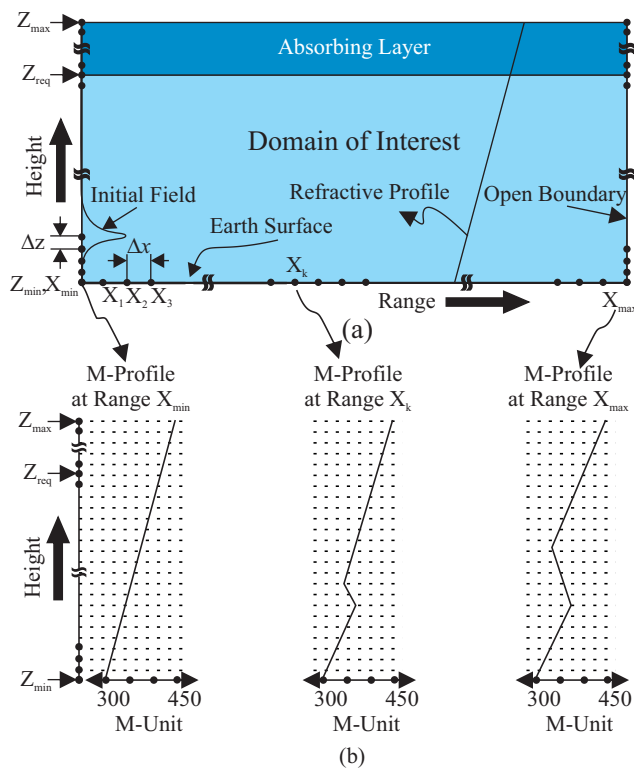


Fig. 1. (a) Geometry of the problem for radio wave propagation modeling (b) Refractivity profiles at specified ranges.

Absorbing Boundary Conditions

For absorbing boundary conditions, the maximum height of problem domain is infinite but only finite height can be handled with numerical methods. Truncation of the domain at finite height can cause strong artificial reflections. In order to stop these non-physical reflections, an absorbing layer, either perfectly matched layer (PML) termination, or non-local boundary condition (NLBC) is used [29], [1]. The absorbing layer in turn is implemented via adding a complex part to the refractive index or by using a window function.

A simple but effective filter is given by the Hanning window of the form of [1]

$$w_h(t) = \frac{1 + \cos(\pi t)}{2} \quad (3)$$

The Hanning window provides a smooth absorptive properties, since, $w_h(0) = 1$ and $w_h(1) = 0$, the derivative at the end points are zero. To make the absorption layers effective, the ratio of absorbing layer height and range increment need to be maximized. More details on domain truncation can be found in [1]. In this work, both complex part to the refractive index and window function is used to truncate the domain above 'domain of interest'.

3. Split-Step Wavelet Method

The SSWM methods have relatively same features as WGM [23] in discretizing altitude operator. However, in terms of the numerical implementation and boundary handling, both algorithms are different when applied to radio wave propagation modeling. The major difference between the SSWM and WGM is that SSWM uses image theory method with periodic wavelet functions, whereas WGM uses the fictitious domain approach with non-periodic wavelet functions. In the formulation of split-step wavelet method, the geometry of problem is modified by using image theory as shown in Fig. 2.

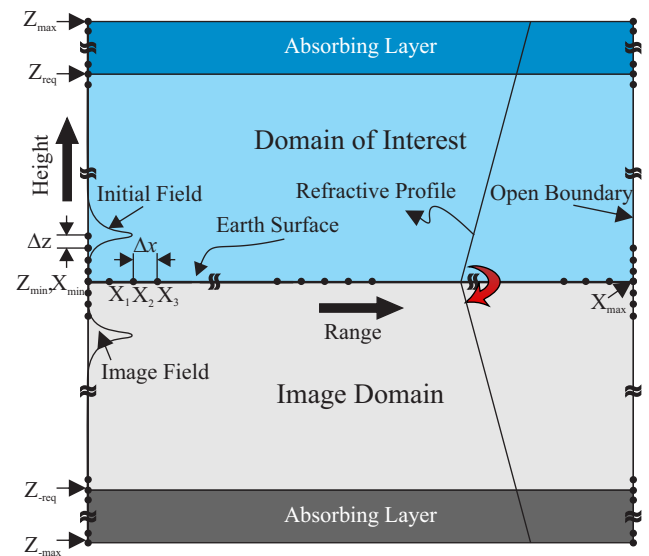


Fig. 2. Solution domain for SSWM.

Now the domain of integration with respect to z is changed from $[0 \ Z_{max}]$ to $[Z_{-max} \ Z_{max}]$. Due to symmetric extension of field and absorbing layer, we can write

$$u(x, Z_{-max}) = u(x, Z_{max}) \approx 0. \quad (4)$$

The equation mentioned above satisfies the definition of periodic boundary condition and it allows us to use integration over the whole z axis. However, due periodicity we can restrict to spatial domain to the interval $[Z_{-max} \ Z_{max}]$.

Let us define the wavelet expansion for unknown function $u(x, z)$ in discrete form as

$$u(x, z) = \sum_{l=0}^{N_z-1} a_l(x)\varphi(z-l); z \in [Z_{-\max}, Z_{\max}] \quad (5)$$

where $a_l(x)$ are the unknown coefficient, $\varphi(z)$ the scaling function. In a fashion similar to WGM we obtain

$$\int_{Z_{-\max}}^{Z_{\max}} \varphi_k \left(\frac{\partial^2 u}{\partial z^2} + 2jk_0 \frac{\partial u}{\partial x} + k_0^2 (m^2 - 1) u \right) dz = 0. \quad (6)$$

After substituting the wavelet expansion of $u(x, z)$ into (6) and rearranging, we have

$$\begin{aligned} \sum_l \frac{\partial a_l(x)}{\partial x} \int_{Z_{-\max}}^{Z_{\max}} \varphi_k \varphi_l dz + \sum_l a_l(x) \frac{-j}{2k_0} \int_{Z_{-\max}}^{Z_{\max}} \varphi_k \frac{\partial^2 \varphi_l}{\partial z^2} dz \\ + \sum_l a_l(x) \frac{-jk_0}{2} \int_{Z_{-\max}}^{Z_{\max}} (m^2 - 1) \varphi_k \varphi_l dz = 0. \end{aligned} \quad (7)$$

In matrix notation, (7) can be written as

$$[I_{k,l}] \{ \partial a_l(x) / \partial x \} + [L_{k,l} + S_{k,l}] \{ a_l(x) \} = 0 \quad (8)$$

where

$$\begin{aligned} I_{k,l} &= \delta_{k,l} = \int_{Z_{-\max}}^{Z_{\max}} \varphi_k \varphi_l dz, \\ L_{k,l} &= \frac{-j}{2k_0} \int_{Z_{-\max}}^{Z_{\max}} \varphi_k \frac{\partial^2 \varphi_l}{\partial z^2} dz = \frac{-j}{2k_0} \left(\Omega_l^{0,2} \right), \\ S_{k,l} &= -\frac{jk_0}{2} \int_{Z_{-\max}}^{Z_{\max}} (m^2 - 1) \varphi_k \varphi_l dz, \end{aligned}$$

$\delta_{k,l}$ is known as Kronecker delta function and $\Omega_l^{0,2}$ are the connection coefficient as described in previous sections. By considering the modified refractivity constant over an element, $S_{k,l}$ can be written as [30],

$$S_{k,l} = -\frac{jk_0}{2} (m^2 - 1) \int_{Z_{-\max}}^{Z_{\max}} \varphi_k \varphi_l dz. \quad (9)$$

The problem given in (7) is an initial value problem. The split-step method derives from the fact that the solution of problem (7) satisfies the identity

$$\{ a_l(x + \Delta x) \} = \exp(L + S) \Delta x \{ a_l(x) \}. \quad (10)$$

The exponential operator given in (10) can be split in two different ways, either

$$\{ a_l(x + \Delta x) \} = \exp(L \Delta x) \exp(S \Delta x) \{ a_l(x) \} \quad (11)$$

called asymmetric splitting or

$$\{ a_l(x + \Delta x) \} = \exp\left(L \frac{\Delta x}{2}\right) \exp(S \Delta x) \exp\left(L \frac{\Delta x}{2}\right) \{ a_l(x) \} \quad (12)$$

called symmetric splitting. It has been shown in [31] that the asymmetrical splitting is accurate to the order $O(\Delta x^2)$ while the symmetrical splitting is accurate to the order $O(\Delta x^3)$. More details on splitting the exponential operator. On the other hand, the accuracy of altitude operator is associated with the moments (M) of the chosen wavelet. In this formulation we are going to use asymmetric splitting and 3rd order moment Daubechies wavelets.

As $S_{k,l}$ is diagonal matrix, the exponential of $S_{k,l}$, required in (12), can be solved cheaply. However, since $L_{k,l}$ is not a diagonal matrix, instead it is a circulant matrix, there is a need to compute the exponential of operator $L_{k,l}$. Let,

$$P = e^Q; Q = L \Delta x / 2. \quad (13)$$

By using the fact that $L_{k,l}$ is circulant, one can compute (13) using FFT as [22]

$$P = \mathcal{F}^{-1} \exp(\Lambda_q) \mathcal{F} \quad (14)$$

where $\Lambda_q = \text{diag}(\hat{q})$, $\hat{q} = \mathcal{F}q$ and q is first column in Q matrix, and \mathcal{F} is FFT.

4. Numerical Implementation of SSWM

In the formulation of SSWM, it was explained that the domain of computation is assumed to be periodic in an interval $[Z_{-\max}, Z_{\max}]$. The matrices given in (8) should be scaled according to physical space. A detailed procedure for physical space mapping of differentiation matrix is given in the Section 7.4 of [22]. If the whole domain is divided in to N_z number of grids points then the indices $l = k = 0, \dots, N_z - 1$ and the dimensions of resultant linear system of (8) will be $N_z \times N_z$. The matrices in (8) will have a following structure for Daubechies wavelet of length 6

$$L_{k,l} = \frac{1}{(2Z_{\max})^2} \begin{bmatrix} \Omega_0^{0,2} & \Omega_{-1}^{0,2} & \dots & \Omega_{-4}^{0,2} & \dots & \Omega_4^{0,2} & \dots & \Omega_1^{0,2} \\ \Omega_1^{0,2} & \Omega_0^{0,2} & \dots & \Omega_{-3}^{0,2} & \dots & 0 & \dots & \Omega_2^{0,2} \\ \vdots & \vdots \\ \Omega_4^{0,2} & \Omega_3^{0,2} & \dots & \Omega_0^{0,2} & \dots & 0 & \dots & 0 \\ 0 & \Omega_4^{0,2} & \dots & \Omega_1^{0,2} & \dots & 0 & \dots & 0 \\ \vdots & \vdots \\ 0 & 0 & \dots & 0 & \dots & \Omega_1^{0,2} & \dots & \Omega_{-4}^{0,2} \\ \Omega_{-4}^{0,2} & 0 & \dots & 0 & \dots & \Omega_0^{0,2} & \dots & \Omega_{-3}^{0,2} \\ \vdots & \vdots \\ \Omega_{-1}^{0,2} & \Omega_{-2}^{0,2} & \dots & 0 & \dots & \Omega_3^{0,2} & \dots & \Omega_0^{0,2} \end{bmatrix}_{N_z \times N_z}$$

$$S_{k,l} = \text{diag} \begin{bmatrix} S_{0,0} \\ \vdots \\ S_{N_z-1, N_z-1} \end{bmatrix}_{N_z \times N_z}, \quad I_{k,l} = [I]_{N_z \times N_z}$$

and

$$a_l(z) = [a_0 \quad \dots \quad a_{N_z-1}]^T_{N_z \times 1}.$$

A symmetric extension of refractive profile is taken in extended region at bottom, as shown in Figure 3.3. We can write

$$S_{\hat{k}, \hat{l}} = S_{k,l}; k, l = (\frac{N_z}{2}), \dots, N_z-1; \hat{k}, \hat{l} = (\frac{N_z}{2} - 1), \dots, 0. \quad (15)$$

Similarly, the initial field is computed at $x = 0$. To satisfy the boundary condition over perfectly conducting surfaces in SSWM, unknown coefficients ($\{a_l(x)\}$) are computed for Dirichlet and Neumann BCs in accordance with image theory. Computational cost can be reduced by using discrete sine or cosine transforms (DST or DCT) for Dirichlet and Neumann BCs, respectively. Since, SSWM is inspired from SSFM, boundary handling cannot be done using conventional methods like fictitious domain approach and capacitance matrix method [21], [32], [33], [32], [23]. At this stage, no other method is available for handling the finite boundary conditions in SSWM. In order to account of finitely conductive surfaces, boundary handling is inspired from DMFT that was basically developed for SSFM to incorporate the impedance boundary conditions.

4.1 Discrete Mixed Fourier Transform (DMFT)

DMFT is basically developed to incorporate the boundary condition in the solution of SSFM [34]. An overview of DMFT formulation is given as follows:

Let us define an auxiliary function $w(x, z)$ for impedance boundary condition given in (2) by

$$w(x, z) = \frac{\partial u(x, z)}{\partial z} + \alpha u(x, m\Delta z) \quad 0 \leq z \leq \infty. \quad (16)$$

Backward difference formula is used to solve (16). The discrete form of (16) can be written as

$$w(x, m\Delta z) = \frac{u(x, m\Delta z) - u[x, (m-1)\Delta z]}{\Delta z} + \alpha u(x, m\Delta z) \quad (17)$$

where $m = 1 \dots N-1$, with $w(x, 0) = w(x, N\Delta z) = 0$ and Δz is the grid size for height operator. Let $r = (1 + \alpha\Delta z)^{-1}$. Equation (17) can be written as

$$w(x, m\Delta z) = u(x, m\Delta z) - r[u(x, (m-1)\Delta z)] \quad (18)$$

where, $m = 1 \dots N-1$. DST of $w(x, m\Delta z)$ yields

$$W(x, g\Delta p) = \sum_{m=1}^{N-1} w(x, m\Delta z) \sin \frac{gm\pi}{N}. \quad (19)$$

Inverse DST of $W(x, g\Delta p)$ is given by

$$w(x, m\Delta z) = \frac{2}{N} \sum_{g=1}^{N-1} W(x, g\Delta p) \sin \frac{gm\pi}{N}. \quad (20)$$

Solution of (16) is given by

$$u(x, m\Delta z) = u_p(x, m\Delta z) + A(x)r^m. \quad (21)$$

Where the particular solution $u_p(x, m\Delta z)$ can be found by setting $u_p(0) = 0$ and using

$$u_p(x, m\Delta z) = w(x, m\Delta z) + ru_p[x, (m-1)\Delta z]. \quad (22)$$

To completely specify the backward difference DMFT, the coefficient $A(x)$ can be computed as

$$A(x) = C(x) - G \sum_{m=0}^N r^m u_p(x, m\Delta z), \quad (23)$$

$$C(x) = \sum_{m=0}^N u(x, m\Delta z) r^m, \quad (24)$$

$$G = \frac{2(1-r^2)}{(1+r^2)(1-r^{2N})}. \quad (25)$$

\sum' indicates that the $m = 0$ and $m = N$ are weighted with a factor of 1/2. The detailed formulation of DMFT can be found in [34], [35].

4.2 Use of DMFT Algorithm in SSWM

The step by step procedure to implement the DMFT is given as follows:

- (1) Compute the coefficients $a_l(0, z)$ using initial field [23].
- (2) Construct the discrete auxiliary function $w(x, m\Delta z)$ using (18).
- (3) Perform DST of $w(x, m\Delta z)$ to compute $W(x, g\Delta p)$.
- (4) Compute free space propagation using procedure given in (14) and extract one side of field.
- (5) Multiply the free space propagator to obtain $W(x + \Delta x, g\Delta p)$.
- (6) The coefficients $C(x)$ must also be propagated to the new range step

$$C(x + \Delta x) = C(x) \exp \left[i\Delta x \sqrt{k_0^2 + \left(\frac{\ln r}{\Delta z} \right)^2} \right].$$
- (7) Perform the Inverse DST to obtain $w(x + \Delta x, m\Delta z)$.
- (8) Solve for $u(x + \Delta x, m\Delta z)$ using (21)-(23).
- (9) Finally, multiply the field distribution $u(x + \Delta x, m\Delta z)$ with environment propagator.
- (10) Repeat step 2 to 9, until maximum required range achieved.
- (11) After reaching the required range step, the required coefficients will be extracted from the extended domain solution.

It should be noted that, for perfectly conducting surfaces, DCT or DST can be used for vertical or horizontal polarized initial field respectively.

In summary, overall algorithm for SSWM implementation is given in Fig. 3.

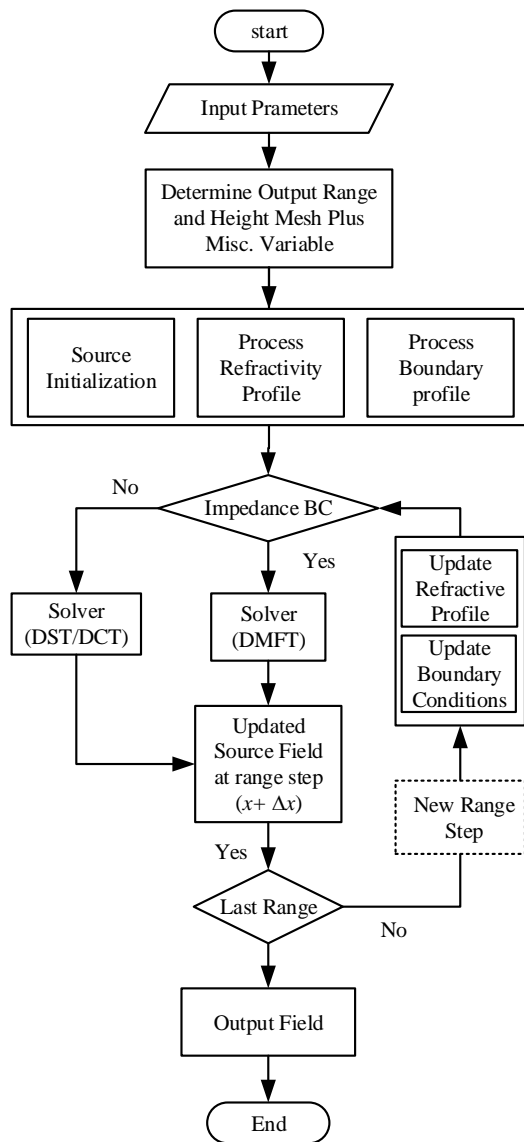


Fig. 3. SSWM Implementation Algorithm for PWE.

5. Results and Discussion

Simulation Experiments:

To illustrate the performance of proposed wavelet based techniques, three major types of numerical experiments, similar to [23], are performed to estimate the path loss in troposphere.

- In the first experiment, we take case of commonly available standard environment condition with Perfectly Electrical Conducting (PEC) BC. Though earth

is not PEC but for high conductive surfaces e.g. water it is justified.

- Second, we have chosen a case of propagation over water. Since, the evaporation duct exists almost all of the time, it is important to predict the behavior of radio wave propagation to design an effective maritime communication system. A detailed study is performed to examine the effect of evaporation duct height and antenna height.

SSWM results are validated by comparing with those of SSFM and WGM [23]. The testing performed here is just to show that the particular implementation of the SSWM, for modeling and simulation of tropospheric radio wave propagation, is valid and the models are suitable for their intended purpose within reasonable bound of accuracy. To show the relative difference between SSWM results and published techniques, Mean Relative Squared Difference (MRSD) is computed for each case with SSFM and WGM data. The formula used to calculate MRSD is given by [36],

$$MRSD = \frac{1}{n} \sum_{i=0}^k \left(\frac{(SSFM \text{ or } WGM \text{ Data}_i) - (SSWM \text{ Data}_i)}{SSFM \text{ or } WGM \text{ Data}_i} \right)^2 \tag{26}$$

5.1 Test Case 1: Propagation over Perfectly Electrical Conducting Earth Surface in Standard Environment

Simulation Setup:

In the first case, path loss results for 100 km transmission range over Perfectly Electrical Conducting (PEC) earth surface are obtained for standard environment at 5.8 Ghz. A refractivity profile used in this simulation is specified by a linear function as [37]

$$M(z) = 326.615 + 0.121433z, \quad 0 \leq z \leq 100 \tag{27}$$

where z is measured in meters. Horizontally polarized transmitter antenna height is chosen at 25 m above the ground level. Beam-width is set to be 3 degrees. The vertical grid size is taken 0.054 m. The range increment is taken to be 125 m for SSFM and SSWM, and 1 m for WGM. The range increment for WGM is taken to be very small to avoid numerical oscillation problems [12]. The bottom boundary is assumed to be perfectly conducting flat earth surface. All simulations for SSWM and WGM are carried out with Daubechies wavelet of length 6. The parameters used in this simulation are summarized in Tab. 1.

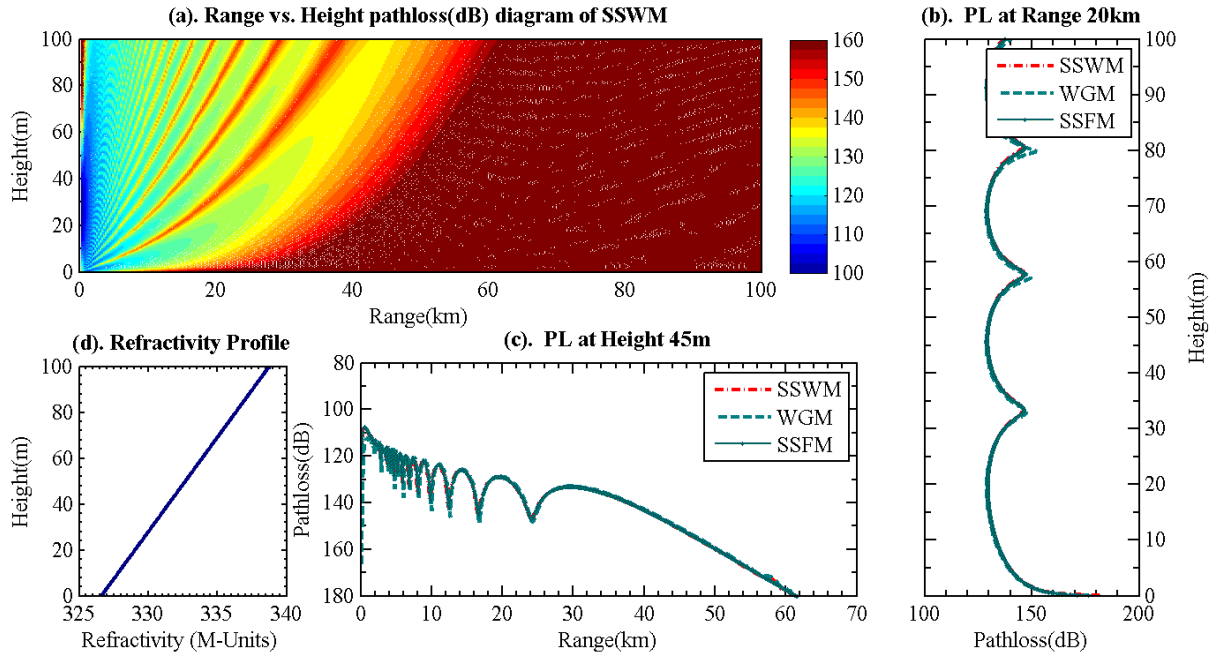


Fig. 4. (a) Range (km) vs. height (m) path loss (dB) diagram for standard environment. (b) Path loss vs. height for range of 20 km. (c) Path-loss vs. range for height of 45 m. (d) Standard environment refractive profile.

Parameter		Value
Frequency		5.8 GHz
Transmission range		100 km
Maximum height		100 m
Altitude grid size (Δz)		0.054 m
Range grid size Δx	SSFM, SSWM	125 m
	WGM	1 m
Antenna height		25 m
Beamwidth		3°
Bottom boundary		PEC
Wavelet Class	SSWM, WGM	Daubechies wavelet (D=6)

Tab. 1. Simulation parameters for propagation over PEC Earth surface in standard environment.

Discussion:

A 3D coverage map of height versus range propagation path loss (dB) over flat earth surface is shown in Fig. 4 (a). In Fig. 4 (a), the results from SSWM are presented and the results from other methods are used only for detailed comparison. The color code bar on the right side of Fig. 4 (a) shows the range of path loss (dB), i.e. [100 160]. For detailed comparison between developed technique, SSFM and WGM, the path loss data are extracted from the results obtained using different numerical schemes for the specific range and height and presented in Fig. 4 (b) and (c). Environment profile is shown in Fig. 4 (d).

From Fig. 4 (a), it can be seen that, for the case of standard refractivity gradient, energy moves away from the earths surface and the radio horizon is only few kilometers. Due to this, energy attenuates fast and beyond the horizon communication becomes a challenging task. A comparison

of propagation path loss results at range 20 km is shown in Fig. 4 (b). The results from both SSWM show a very good match with those from SSFM and WGM. Fig. 4 (c) illustrates the comparison of path loss versus range at height 45 m. A strong interference and deep nulls can be seen for the first few kilometers because of the reflections from the earth surface. This region is normally referred to as interference region. After 30 km, or beyond the horizon, the attenuation slope is very high. In this region, the major part of energy comes from the diffraction phenomenon. Due to this, it is referred to as diffraction region. In diffraction region, the attenuation reaches approximately 200 dB for standard environment. Therefore, a good communication after few kilometers is not possible for low altitude receiver antenna heights. Communication range can only be increased by increasing the altitude of our receiver or transmitter antenna.

For performance evaluation of the newly developed techniques SSWM, the MRSD is computed using (26) for the cases given in Fig. 4 (b) and (c). It is found that the MRSD is of the order of 10^{-5} , the detail of MRSD results is presented in Tab. 4.

It is also observed that, for large range increment sizes,

SSWM can produce good results while WGM suffers from oscillation problem, due to which the range increment size for WGM is taken quite small compared to SSWM. It is also observed that SSWM is about 18 times faster then WGM and the computation cost of SSWM is no different from that of SSFM and being a sub-domain solution, SSWM takes all advantages of WGM, as shown in Tab. 5.

5.2 Test Case 2: Propagation in Evaporation Duct over Finite Conductive Earth Surface

Simulation Setup:

This simulation is performed over finite conductive sea surface using 10.5 GHz. And we demonstrated the behavior of radio wave propagation in evaporation duct as shown in Fig. 5. The evaporation duct profile used in this simulation is given in Tab. 2. Simulations were carried out with horizontally polarized transmitter antenna with 15 m height above the ground level. Beam-width is set to be 2 degrees. The vertical grid size is taken 0.054 m. The range increment is 125 m for SSFM and SSWM and 1 m for WGM. The bottom boundary is assumed to be finitely conducting flat sea surface. The parameters used in this simulation are summarized in Tab. 3.

Height (m)	M-Units
0	357.021
0.135	334.332
0.223	332.730
0.368	331.169
0.607	329.673
1	328.273
1.649	327.007
2.718	325.920
4.482	325.061
7.389	324.488
11.76	324.293
12.182	324.294
20.086	324.623
33.115	325.720
54.598	328.010
100	332.186

Tab. 2. Refractive profile for evaporation duct.

Discussion:

Once more, a comparison between results is presented. In Fig. 5 (a), 3D converge map using SSWM shows the strong trapping of signals in evaporation duct. Fig. 5 (b) and (c) shows the detailed comparison of AREPS and from SSWM and WGM data at specified range and height. Fig. 5 (b) illustrates the path loss versus height at range 35 km while Fig. 5 (c) shows the path loss versus range at height 15 m. Environment profile used in this simulation is shown in Fig. 5 (d).

Again, for performance evaluation, MRSD is computed for SSWM using (26) for the cases given in Fig. 5 (b) and (c). Results given in Tab. 4 show that MRSE is of the order of 10^{-4} . Hence, a very good agreement between the results is

found. Similar to previous case, the range increment size for SSWM is quite large compared to WGM. Therefore, SSWM saved much more computation time as compared to WGM while the computation cost of SSWM is similar to SSFM. The summary of computation cost for all test cases is given in Tab. 5.

Parameter		Value
Frequency		10.5 GHz
Transmission range		100 km
Maximum height		100 m
Altitude grid size (Δz)		0.054 m
Range grid size Δx	SSFM, SSWM	125 m
	WGM	1 m
Antenna height		15 m
Beamwidth		2°
Bottom boundary		Sea Surface
Wavelet Class	SSWM, WGM	Daubechies wavelet (D=6)

Tab. 3. Simulation parameters for propagation in evaporation duct over finite conductive Earth surface.

From Fig. 5 (a), it can also be seen that the radio waves are highly affected by this natural waveguide. In this case too, the same regions of interference, diffraction and troposcatter are present as in surface duct. In Fig. 5 (b), it can be observed that the propagation path loss is about 140 dB at observation height of 4 m and remains very stable for long distances. Fig. 5 (c) also shows another interesting feature of evaporation duct that, unlike previous cases, the interference region is shrunken to few kilometers and a very smooth attenuation can be observed with a rate much less than standard atmosphere. It also indicates that evaporation duct can be suitable for radio links using receiver antenna at few meters altitude. As the percentage occurrence of evaporation duct is more frequent as compared to surface-based and elevated duct.

Test Case	MRSD w.r.t.			
	SSFM		WGM	
	Range	Height	Range	Height
1	3.2×10^{-03}	1.2×10^{-05}	3.6×10^{-04}	1.1×10^{-04}
2	8.1×10^{-05}	1.0×10^{-04}	1.2×10^{-04}	5.1×10^{-05}

Tab. 4. Summary of MRSE results.

Test Case	Computation Time (Sec)		
	SSWM	SSFM	WGM
1	8.71	7.21	149.57
2	8.62	7.23	150.44

Tab. 5. Comparison of computation time for SSWM, SSFM and WGM.

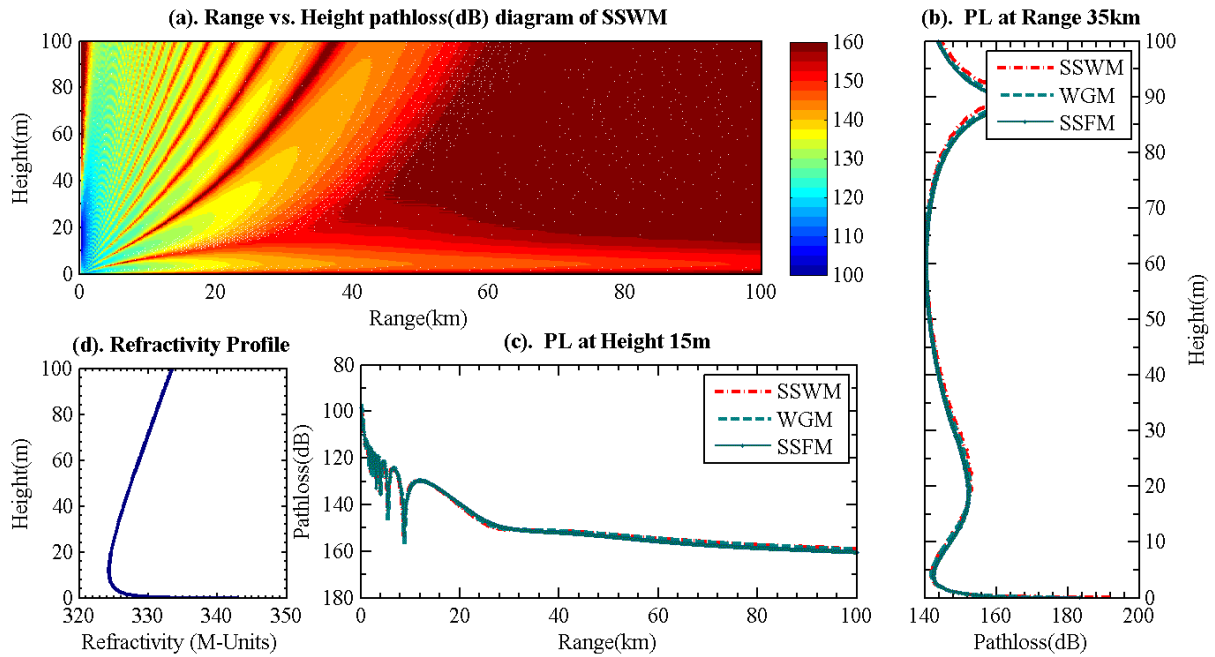


Fig. 5. (a) Range (km) vs. height (m) path loss (dB) diagram for evaporation duct. (b) Path loss vs. height for range of 35 km. (c) Path-loss vs. range for height of 15 m. (d) Evaporation duct refractive profile.

It can be observed from Tab. 5, the computation time for SSWM and SSFM is almost same. However, SSWM has better localization properties as compared to SSFM where the basis functions are entire-domain functions. Sub-domain basis functions gives us the opportunity to handle discontinuities more efficiently with same computational load while Fourier solutions may require very high order of harmonics to achieve the similar accuracy. It is also possible to extend sub-domain solution to adaptive gridding which may not possible in Fourier based solutions. The feasibility of SSWM for PWE also opens the door for hierarchical solutions for desired level of accuracy with less computations cost as compared to other finite element or difference methods.

6. Conclusion

In this paper, an improved SSWM is presented for the numerical solution of two dimensional PWE. It incorporate DCT/DST and DMFT for PEC and non-PEC boundary conditions respectively. The performance of SSWM is demonstrated for standard and ducting environment conditions and results were compared with those from AREPS. A strong agreement is found for all environment conditions. From results, it is also found that unlike other sub-domain solutions, the proposed method not only allows larger range steps but it also provides more accurate solution almost as fast as SSFM. In conclusion, this work can be a significant step towards the improvement of propagation model to predict the anomalous propagation in troposphere.

References

- [1] LEVY, M. *Parabolic Equation Methods for Electromagnetic Wave Propagation*. Inst. of Engineering & Technology, 2000.
- [2] LEONTOVICH, M., FOCK, V. Solution of the problem of propagation of electromagnetic waves along the Earth's surface by the method of parabolic equation. *Acad. Sci. USSR. J. Phys*, 1946, vol. 10, p. 13–24.
- [3] KO, H., SARI, J., THOMAS, M., HERCHENROEDER, P., MARTONE, P. Anomalous propagation and radar coverage through inhomogeneous atmospheres. *AGARD Characteristics of the Lower Atmosphere Influencing Radio Wave Propagation 14 p(SEE N 84-24943 15-32)*, 1984.
- [4] CLAERBOUT, J. *Fundamentals of Geophysical Data Processing*. New York: McGraw Hill, 1975.
- [5] CLAYTON, R., ENGQUIST, B. Absorbing boundary conditions for acoustic and elastic wave equations. *Bulletin of the Seismological Society of America*, 1977, vol. 67, no. 6, p. 1529–1540.
- [6] COLE, J. Modern developments in transonic flow. *SIAM Journal on Applied Mathematics*, 1975, vol. 29, no. 4, p. 763–787.
- [7] HASEGAWA, A., TAPPERT, F. Transmission of stationary nonlinear optical pulses in dispersive dielectric fibers. i. anomalous dispersion. *Applied Physics Letters*, 1973, vol. 23, no. 3, p. 142–144.
- [8] TAPPERT, F., HARDIN, R. Application of the split-step Fourier method to the numerical solution of nonlinear and variable-coefficient wave equations. *SIAM Review*, 1973, vol. 15, p. 423.
- [9] COOLEY, J., TUKEY, J. An algorithm for the machine calculation of complex Fourier series. *Mathematics of Computations*, 1965, vol. 19, no. 90, p. 297–301.
- [10] SINGLETON, R. An algorithm for computing the mixed radix fast Fourier transform. *IEEE Transactions on Audio and Electroacoustics*, 1969, vol. 17, no. 2, p. 93–103.

- [11] OPPENHEIM, A., WEINSTEIN, C. Effects of finite register length in digital filtering and the fast Fourier transform. *Proceedings of the IEEE*, 1972, vol. 60, no. 8, p. 957-976.
- [12] ISAAKIDIS, S., XENOS, T. Parabolic equation solution of tropospheric wave propagation using FEM. *Progress In Electromagnetics Research*, 2004, vol. 49, p. 257-271.
- [13] DESHPANDE, V., DESHPANDE, M. Study of electromagnetic wave propagation through dielectric slab doped randomly with thin metallic wires using finite element method. *IEEE Microwave and Wireless Components Letters*, 2005, vol.15, no. 5, p. 306-308.
- [14] ORAIZI, H., HOSSEINZADEH, S. A novel marching algorithm for radio wave propagation modeling over rough surfaces. *Progress In Electromagnetics Research*, 2006, vol. 57, p. 85-100.
- [15] ARSHAD, K., KATSRIKU, F., LASEBAE, A. An investigation of wave propagation over irregular terrain and urban streets using finite elements, *Proceedings of the 6th WSEAS Int. Conference on Telecommunications and Informatics*, 2007, p. 105-110.
- [16] APAYDIN, G., SEVGI, L. Numerical investigations of and path loss predictions for surface wave propagation over sea paths including hilly island transitions. *IEEE Transactions on Antennas and Propagation*, 2010, vol. 58, no. 4, p. 1302-1314.
- [17] MEHRA, M., KEVLAHAN, N. An adaptive wavelet collocation method for the solution of partial differential equations on the sphere. *Journal of Computational Physics*, 2008, vol. 227, no. 11, p. 5610-5632.
- [18] DAUBECHIES, I. Orthonormal bases of compactly supported wavelets. *Communications on Pure and Applied Mathematics*, 1988, vol. 41, no. 7, p. 909-996.
- [19] GLOWINSKI, R., LAWTON, W., RAVACHOL, M., TENENBAUM, E. Wavelet solutions of linear and nonlinear elliptic, parabolic and hyperbolic problems in one space dimension. *Computing Methods in Applied Sciences and Engineering*, 1990, p. 55-120.
- [20] LIANDRAT, J. *Resolution of the 1D regularized burgers equation using a spatial wavelet approximation*, ICASE Report No. 90-83 , 1990.
- [21] AMARATUNGA, K., WILLIAMS, J., QIAN, S., WEISS, J. Wavelet-Galerkin solutions for one dimensional partial differential equations. *International Journal for Numerical Methods in Engineering*, 1994, vol. 37, no. 16, p. 2703-2716.
- [22] NIELSEN, O. *Wavelets in Scientific Computing*. Ph.D. thesis. Informatics and Mathematical Modelling, Technical University of Denmark, 1998.
- [23] IQBAL, A., JEOTI, V. A novel wavelet-Galerkin method for modeling radio wave propagation in tropospheric ducts. *Progress In Electromagnetics Research B*, 2012, vol. 36, p. 35-52.
- [24] PIERCE, I., WATKINS, L. Modelling optical pulse propagation in nonlinear media using wavelets. *Proceedings of the IEEE-SP International Symposium on Time-Frequency and Time-Scale Analysis*, 1996, p. 361-363.
- [25] PASKYABI, M. B., RASHIDI, F. Split step wavelet Galerkin method based on parabolic equation model for solving underwater wave propagation. *In Proceedings of the 5th WSEAS International Conference on Wavelet Analysis and Multirate Systems*, USA, 2005, p. 1-7.
- [26] LANDOLSI, T. Accuracy of the split-step wavelet method using various wavelet families in simulating optical pulse propagation. *Journal of the Franklin Institute*, 2006, vol. 343, no. 4-5, p. 458-467.
- [27] IQBAL, A., JEOTI, V. A split step wavelet method for radiowave propagation modelling in tropospheric ducts. *2011 IEEE International RF and Microwave Conference*, 2011, p. 67-70.
- [28] IQBAL, A., JEOTI, V. Numerical modeling of radio wave propagation in horizontally inhomogeneous environment using split-step wavelet method. *In 4th International Conference on Intelligent and Advanced Systems (ICIAS)*, 2012, p. 200-205.
- [29] ANTOINE, X., ARNOLD, A., BESSE, C., EHRHARDT, M., SCHDLE, A. A review of transparent and artificial boundary conditions techniques for linear and nonlinear schrodinger equations. *Communications in Computational Physics*, 2008, vol. 4, no. 4, p. 729-796.
- [30] SIRKOVA, I., MIKHALEV, M. Parabolic wave equation method applied to the tropospheric ducting propagation problem: a survey. *Electromagnetics*, 2006, vol. 26, no. 2, p. 155-173.
- [31] KREMP, T. *Split-step wavelet collocation methods for linear and nonlinear optical wave propagation*. Ph.D. thesis, Institute of Photonics and Quantum Electronics, Karlsruhe Institute of Technology, 2002.
- [32] QIAN, S., WEISS, J. Wavelets and the numerical solution of partial differential equations. *Journal of Computational Physics*, 1993, vol. 106, no. 1, p. 155-175.
- [33] LU, D., OHYOSHI, T., ZHU, L. Treatment of boundary conditions in the application of wavelet-Galerkin method to an SH wave problem. *International Journal of the Society of Materials Engineering for Resources*, 1997, vol. 5, no. 1, p. 15-25.
- [34] KUTTLER, J., DOCKERY, G. An improved-boundary algorithm for Fourier split-step solutions of the parabolic wave equation. *IEEE Transactions on Antennas and Propagation*, 1996, vol. 44, no. 12, p. 1592-1599.
- [35] KUTTLER, J., JANASWAMY, R. Improved Fourier transform methods for solving the parabolic wave equation. *Radio Science*, 2002, vol. 37, no. 2, p. 1021.
- [36] BALAGURUSAMY, E. *Numerical Methods*. New Delhi: Tata McGraw-Hill Pub.Co.Ltd, 1999.
- [37] JANASWAMY, R. *A Rigorous Way of Incorporating Sea Surface Roughness Into the Parabolic Equation*, PN, 1995.

About Authors...

Asif IQBAL received his M.Sc. degree in Electrical & Electronics Engineering from Universiti Teknologi Petronas, Malaysia in 2012. Currently, he is full time Ph.D. student at Department of Electrical and Electronics Engineering, Universiti Teknologi Petronas, Malaysia. His research interest include fast and efficient numerical algorithms, radio propagation, wireless channel characterization and modelling. He is currently working on the channel sounder and emulators.

Varun JEOTI received his Ph.D. degree from Indian Institute of Technology Delhi India in 1992. He worked on several sponsored R&D projects in IIT Delhi and IIT Madras during 1980 to 1989. He was a Visiting Faculty in Electronics department in Madras Institute of Technology, Anna University for about 1 year from 1989 to 1990 and joined Delhi Institute of Technology for next 5 years till 1995. He moved to Electrical & Electronic Engineering school of Universiti Sains Malaysia in 1995 and joined Electrical & Electronic Engineering department of Universiti Teknologi PETRONAS in 2001. His research interests are in the area of signal processing, surface acoustic wave (SAW) devices, wireless SAW sensor network and wireless communication for maritime applications besides others.